N72-10061

EXPERIMENTAL AND COMPUTER STUDIES OF THE RADIATION EFFECTS IN SILICON SOLAR CELLS*

R. E. Leadon, J. A. Naber, and B. C. Passenheim
Gulf Radiation Technology
San Diego, Calif.

I. INTRODUCTION

This paper is presented in two parts. The first section will be a summary of selected experimental results obtained on lithium-diffused bulk silicon. Particular emphasis was placed on the radiation-induced degradation and thermal anneal of minority-carrier in bulk silicon because solar cell output is related to the minority-carrier lifetime. The temperature dependence of the minority-carrier lifetime indicates the density and energy levels of the recombination centers, providing clues to their identity. Electron spin resonance and infrared absorption techniques were used to investigate the introduction and anneal of three specific radiation-induced defects, which are thought to contribute to the recombination process.

The results reported herein are a continuation and summary of work previously reported (Refs. 1-8).

The second part of the paper will discuss the merits of a computer code developed by Gulf Radiation Technology which calculates the current-voltage (I-V) output of a computer simulated P-N junction. With this code, the user stipulates the initial properties and environment of a cell. The cell's properties and environment may then be varied in a manner which might reflect the anticipated radiation exposure and mission environment, and the current-voltage output is recalculated. Thus, a variety of cell types and experimental conditions can be rapidly evaluated. This code can also be utilized by cell manufacturers to evaluate the merit of different cell types, doping profiles, and cell parameters. It can be utilized by those engaged in solar cell testing programs to evaluate a greater variety of cell types, radiation histories, and ambient conditions than is feasible by experimental techniques alone. Systems engineers can use the code to predict the radiation vulnerability of solar cells in varied environments.

II. EXPERIMENTAL PROGRAM

A. Samples and Radiation

The experimental program has been devoted to an investigation of bulk lithium-diffused silicon. Electron spin resonance and infrared absorption were used to study certain specific defects, and minority-carrier lifetime measurements were used to study radiation-induced recombination centers. Samples were lithium-diffused by either a lithium-oil paint-on technique or by a lithium-tin bath technique. Samples with lithium donor densities from as low as 2×10^{20} Li/m^3 (2×10^{14} Li/cm^3) to as high as 4×10^{23} Li/m^3 (4×10^{17} Li/cm^3) were investigated. Resistivity profiles were used to monitor samples for diffusion uniformity. Donor density was occasionally verified

*Work performed for the Jet Propulsion Laboratory, sponsored by the National Aeronautics and Space Administration under Contract NAS 7-100.

by Hall effect measurements. Samples were diffused from vacuum float-zone (FZ) and quartz-crucible (QC) phosphorus-doped silicon, ranging in initial room-temperature resistivity from 10^2 Ω-m (10^4 Ω-cm) to 0.005 Ω-m (0.5 Ω-cm). While QC silicon has approximately a hundred times the oxygen concentration of FZ silicon, its dislocation density is much less.

Samples were damaged with 30-MeV electrons at temperatures ranging from 115 to 300 K or by fission neutrons (E > 10 keV) at 273 to 300 K. The damage was thermally annealed at temperatures up to 673 K.

B. Study of Three Specific Defects

The introduction of three specific defects by 30-MeV electron irradiation and their subsequent thermal anneal were investigated using electron spin resonance or infrared absorption techniques. Specifically, the oxygen-vacancy (Si-B1), divacancy (Si-G7), and phosphorus-vacancy (Si-G8) centers have been studied. The results of these studies have been previously reported elsewhere (Refs. 7, 8) but may be summarized as follows.

The oxygen-vacancy and phosphorus-vacancy centers were studied by ESR techniques. In QC silicon, the Si-B1 center introduction rate is the same as in nondiffused silicon ($\sim 15\ m^{-1} = 0.15\ cm^{-1}$) as long as the lithium density is much less than the oxygen density. When the lithium and oxygen densities are comparable, and B1 center introduction rate is significantly reduced ($\sim 2.5\ m^{-1} = 0.025\ cm^{-1}$). This can be attributed to the lithium-oxygen pairing, reducing the number of oxygen atoms available to form oxygen-vacancy (Si-B1) centers, or to competition between oxygen and the positively charged lithium or lithium oxide donors for the vacancies. The B1 center in lithium-diffused silicon is found to anneal below 400 K instead of near 600 K, as in nondiffused silicon. The LiO^+ density and conductivity decreased as the Si-B1 center annealed.

Electron spin resonance was also used to study the phosphorus-vacancy (Si-G8) center. In phosphorus-doped lithium-diffused silicon ($10^{22}\ P/m^3 = 10^{16}\ P/cm^3$, $\sim 10^{22}\ Li/m^3 \cong 10^{16}\ Li/cm^3$), 30-MeV electron irradiations of $10^{21}\ e/m^2$ ($10^{17}\ e/cm^2$) below 150 K are found to produce Si-G8 (phosphorus-vacancy) defects at a rate comparable to nondiffused silicon. Production and annealing studies on the Si-G8 center at these densities and fluence levels indicate that the presence of lithium had little or no effect on the creation or annealing of that center. It is possible that at these high fluences, relative to the initial lithium density, the active lithium has been depleted.

The divacancy (Si-G7) was observed by monitoring the introduction and anneal of the 1.8-μm optical absorption band. In this investigation, it was found that for 30-MeV electron irradiations at less than 150 K to fluences of $10^{21}\ e/m^2$ ($10^{17}\ e/cm^2$), the introduction rate of the Si-G7 center (divacancy) is comparable in electron-irradiated lithium-diffused ($5 \times 10^{22}\ Li/m^3 = 5 \times 10^{16}\ Li/cm^3$) and nondiffused silicon. The divacancy anneals at or below 300 K in diffused silicon compared with ~325 to 575 K in nondiffused silicon. As the 1.8-μm divacancy band disappears, new bands near 1.4 and 1.65 μm appear, and these anneal near 600 K. These bands have been observed by other investigators (Ref. 9) and attributed to the divacancy plus one or two lithium atoms.

C. Minority-Carrier Lifetime Measurements

The introduction and anneal of recombination centers were determined from minority-carrier lifetime measurements. Minority-carrier lifetime was determined from measurements of the decay of photoconductivity or by steady-state techniques. These measurements are described in detail elsewhere (Refs. 3, 8). The present results were at injection levels ($\Delta n/n_0$) of less than 1%. Interpretation of the results is based on Shockley-Read recombination theory (Ref. 10). Capture cross-section temperature dependence as estimated by Lax (Ref. 11) or Leadon (Ref. 12) was assumed. The temperature dependence of minority-carrier lifetime was measured before and after irradiation and again after thermal anneal. Figure 1 shows minority-carrier lifetime versus inverse temperature for a lithium-diffused quartz-crucible and a lithium-diffused float-zone sample. The minority-carrier lifetime temperature dependence of the QC silicon can be attributed to recombination centers further than about 0.3 eV from either band edge, but the lifetime of FZ silicon has a more severe temperature dependence and a discontinuity near $1000/T = 4.5\ K^{-1}$. This can be attributed to recombination centers about 0.17 eV below the conduction band, which were not observed in QC silicon, in addition to centers further than 0.35 eV from either band edge. The lines drawn through the data represent the low injection-level lifetimes calculated by Shockley-Read theory, assuming the temperature-dependent capture cross sections of Lax. The presence of a recombination center near E_c - 0.17 eV in FZ silicon and its absence in QC silicon suggests that this center is not the oxygen-vacancy (Si-B1) center, which is known to have an energy level in this range.

The minority-carrier lifetime degradation rate is defined in terms of lifetime τ and electron fluence ϕ to be

$$K = \frac{\Delta(\tau^{-1})}{\Delta\phi}$$

compared with phosphorus-doped silicon, and was found to increase with increasing lithium donor density. The degradation constant was found to be essentially independent of oxygen content. This shows that the 30-MeV electron-induced defects either contain lithium or are affected in their production by lithium. The minority-carrier lifetime degradation constant was found to vary with temperature in a way which could be attributed to the temperature dependence of the capture cross section.

Both isothermal and isochronal annealing experiments have been performed on a variety of lithium-diffused samples. The unannealed fraction of annealable defects for isothermal annealing is given by

$$\frac{1/\tau_t - 1/\tau_f}{1/\tau_0 - 1/\tau_f}$$

where τ_0 is the lifetime after irradiation and before anneal, τ_f is the fully annealed lifetime, and τ_t is the lifetime at the annealing temperature after time t. Linearity of the isothermal annealing data implies first-order annealing kinetics (Ref. 13) in which the number of recombination centers is given by

$$N = N_0 \exp(-Rt)$$

where N_0 is the initial number of annealable defects and R is the rate constant, which is given by

$$R = \nu \exp(-E/kT)$$

where E is the activation energy and ν is the effective frequency factor. In every case, our isothermal anneals indicated first-order annealing kinetics were appropriate.

For isochronal anneals, the unannealed fraction of annealable defects is given by

$$\frac{1/\tau_T - 1/\tau_f}{1/\tau_0 - 1/\tau_f}$$

where τ_T is the lifetime observed at 300 K after anneal at temperature T, and τ_0 and τ_f are the pre- and post-anneal lifetimes.

Analysis of isochronal and isothermal anneals, using first-order kinetics, yields the activation energy and frequency factor of the rate constant. Figure 2 shows the results of five separate isochronal annealing experiments on lithium-diffused QC silicon. A single first-order annealing stage at 380 ±10 K is readily apparent. Similar results were obtained on fission-neutron-irradiated silicon.

Table 1 summarizes our experimental findings for the annealing of radiation-induced recombination centers in lithium-diffused silicon exposed to 30-MeV electron and fission neutrons ($E > 10$ keV). The activation energies compare with the 0.65 ± 0.05 eV energy for lithium diffusion in oxygen-lean FZ silicon, and with 1.07 ± 0.05 eV energy of lithium-oxygen dissociation and diffusion in oxygen-rich QC silicon (Refs. 14-16). This data supports the supposition that radiation-induced damage, including the clustered damage attributed to fission neutrons, is annealed by the diffusion of lithium to the defect.

In addition, the effective frequency factors are much less than the atomic frequency factor of about 10^{13} s^{-1} and scale with the lithium donor density. This is consistent with a process involving the long-range migration of one annealing species to another (Ref. 13), which we take to be the migration of lithium to the damage site.

A more detailed discussion of our experimental findings and theoretical interpretations is presented elsewhere (Ref. 8), and a considerable body of additional data, provided by us and other investigators using other techniques, is available on bulk silicon. The following section of this paper describes one means of applying this body of data to the problem of predicting the response of a solar cell to various radiation and environmental conditions.

III. CODE FOR PREDICTING PERFORMANCE OF SOLAR CELLS

The purpose of this presentation is to describe a computer program that can be used for predicting the output performance of solar cells. This code was developed under Defense Atomic Support Agency contract and applied to solar cells under the JPL contract. Briefly, this code, which is fully operational at the present time, solves the complete equations for a one-dimensional P-N junction. The code starts with the current and continuity equations for electrons and holes, Poisson's equation for the electric field inside the cell, and appropriate equations for the generation and recombination of excess carriers. Arbitrary one-dimensional space profiles of doping density, mobilities, recombination lifetimes, and ionization densities are inputs to the code. The partial differential equations are converted to finite difference approximations, which are then solved by iteration. In principle, there are no adjustable parameters in the code. If one had accurate values for all of the material properties, the code would predict the absolute magnitudes of the current and voltage for selected values of load resistance. Thus, the accuracy of the results is primarily determined by how well one can measure or estimate the important physical parameters of the cell.

This code could be useful both in the design of new devices and in the analysis of radiation effects to solar cells. For example, if a cell manufacturer is designing a new type of cell, perhaps with an unusual doping profile, he could estimate the performance of the new device relative to a conventional cell and optimize its parameters before he goes through the expense of constructing it. Similarly, the radiation-effects physicist could use such a code to help him analyze his solar cell data in terms of kinds and densities of defects created by the radiation and to extrapolate the results to other radiation environments.

The three basic equations of the code are the one-dimensional continuity equations for holes (p) in the valence band and electrons (n) in the conduction band, and Poisson's equation for the electric field (E).

$$\frac{\partial p(x,t)}{\partial t} = g(x,t) - R(x,t) - \frac{\partial J_p(x,t)}{\partial x} \quad (1)$$

$$\frac{\partial n(x,t)}{\partial t} = g(x,t) - R(x,t) - \frac{\partial J_n(x,t)}{\partial x} \quad (2)$$

$$\frac{\partial E(x,t)}{\partial x} = \frac{q}{K}[p(x,t) - n(x,t) + \Delta N(x)] \quad (3)$$

In the above equations, the dimension x is normal to the face of the cell and $g(x, t)$ is the time- and space-dependent ionization rate of electron-hole pairs by the external radiation. This quantity is calculated ahead of time, using the spectral distribution of the incident light and the attenuation coefficients for the particular material, and is then an input into the code. The quantity q is the magnitude of the electronic charge, K is the dielectric constant in MKS units, $\Delta N(x)$ is the net doping of the semiconductor (positive for n-type, negative for p-type), and J_p and J_n are the particle current densities given by

$$J_p = p\mu_p E - D_p \frac{\partial p}{\partial x} \quad (4)$$

$$J_n = -n\mu_n E - D_n \frac{\partial n}{\partial x} \quad (5)$$

In Eqs. (4) and (5), the first terms are the drift components of the currents with mobilities μ_p and μ_n, while the second terms give the diffusion currents with diffusion coefficients D_p and D_n.

The term $R(x, t)$ is the rate of recombination of excess carriers via recombination centers. There are several different options available to a user, depending on the sophistication he wishes to use in describing the recombination process. In many situations, it is adequate to use a Shockley-Read-type recombination rate for a single recombination level:

$$R = \frac{np - n_i^2}{\tau_{O_n}(p + p_F) + \tau_{O_p}(n + n_F)} \quad (6)$$

where n_i is the intrinsic carrier density, p_F and n_F are the values of p and n when the Fermi level coincides with the level of the recombination center that is being considered, and τ_{O_n} and τ_{O_p} are the recombination lifetimes of electrons in heavily p-type material and of holes in heavily n-type material, respectively.

This recombination equation does have the limitation that it only simulates the simultaneous annihilation of a free electron and a free hole. It does not consider the trapping of carriers on defect centers and, therefore, carrier removal. Since the latter phenomena can be important when the details of the trapping kinetics affect the carrier lifetimes or removal rates, the code also has the capability of simulating both single-level and double-level traps. This could be important, for example, if the radiation produces a high-density region of defect centers which significantly depletes the majority carriers and creates a p-n junction effect.

For a single-level trap with density N_1 and two possible charge states, negative (N_1^-) and neutral (N_1^o), the (-R) term in Eq. (1) would be replaced by

$$-R_p^- = \alpha_p^-\left(pN_1^- - N_1^o p_F\right) \quad (7)$$

and the (-R) term in Eq. (2) would be replaced by

$$-R_n^o = \alpha_n^o\left(nN_1^o - N_1^- n_F\right) \quad (8)$$

The quantity α_p^- is the product of the thermal velocity of a hole in the valance band and the cross section α_p^- for capture of a hole by a negatively charged defect, and α_n^o is a similar term for capture of an electron by a neutral defect. In addition to modifying Eqs. (1) and (2), the density of the negatively charged center (N_1^-) must be included in the summation of charges in Eq. (3). Furthermore, additional equations are required for the rate of change of N_1^- and N_1^o. For constant total N_1,

$$\frac{dN_1^-}{dt} = -\frac{dN_1^o}{dt} = R_n^o - R_p^- \quad (9)$$

Similar equations are available in the code for a double-level defect with three charge states, N_2^-, N_2^o, and N_2^+, but, for brevity, they are not presented here.

To obtain a solution to the above equations, they are converted to finite difference form for some prescribed mesh distribution. The distribution of the meshes can be chosen arbitrarily by the user to most judiciously utilize the permissible number of meshes. On the Univac 1108, core storage limits the number of meshes to about 230, which is an adequate number to simulate a three-layer planar transistor, and is certainly enough for a two-region solar cell.

Since this code was originally developed to study time-dependent processes in semiconductor devices, the finite difference equations are solved by iteration for finite time steps. Under conditions of steady illumination and circuit load, the code quickly goes to the steady-state solution. The resulting steady voltage and current form one point on the I-V curve. Additional points are obtained by changing the external load resistance and again allowing the problem to run to equilibrium.

Since Eqs. (1), (2), and (3) are time-dependent partial differential equations, one must specify boundary conditions at the two ends of the device and self-consistent initial distributions on n, p, and E. The self-consistent initial distributions could have been specified in any number of ways. To simplify the task of the user, a new problem is started from a condition of zero electric field and charge neutrality everywhere. This is usually a physically unrealistic, but mathematically correct, starting point. The code then does the work of proceeding to the correct solution. For a subsequent run, with the same device, it is usually possible and economical to restart from any previous cycle.

Two types of boundary conditions are available. The first, called "bulk," forces the carrier densities at the two ends of the device to have zero slopes. This is the condition that would apply if the p-n junction were far from the contacts

and the densities have a chance to approach their bulk values far from the junction (hence the name "bulk"). This boundary condition is suitable when the details of the contact are not important in the problem.

On the other hand, when the details of the contact between the semiconductor and the metal are important, the contact potential between the two materials can be simulated in the second type of boundary condition. A large surface recombination velocity can be simulated by defining a narrow region at the surface with a very short recombination lifetime. Of course, an additional requirement is that the current through the exterior circuit must equal the current through the device, including the displacement current in time-dependent problems. Detailed descriptions of the starting and operating procedures for the code can be found in Refs. 17 and 18.

Since this code solves the complete equations for the solar cell, the answers that it provides should be as good, within the accuracy of the finite difference method of solution, as the input data supplied to the code. For comparative design studies, the theoretical device characteristics can be specified exactly and the effect of varying one or more parameters individually can be evaluated. For the analysis of radiation effects in an actual device, the problem is somewhat different because the parameters for the undamaged test device, such as doping profile and lifetimes, are usually not accurately known. For the best results, it is always desirable to avail oneself of all possible nondestructive tests to determine the device parameters, such as capacitance-voltage measurements and resistivity for the doping density profile and diffusion lengths for the lifetimes.

However, in the final analysis, it may be necessary to adjust these parameters somewhat by trial and error to obtain acceptable agreement with the preirradiated test data. Once these characteristics are determined for the undamaged cell, the change in the bulk parameters due to radiation damage can then be estimated and included in the code. If the test data on radiation effects in the bulk material are sufficiently good so that the model for the radiation damage and the change per unit dose can be correctly determined, the predicted results for the irradiated cell should be in acceptable agreement with the post-irradiation test data. If there is significant disagreement, it must mean that the model for the radiation damage or the magnitude of the radiation effects is different from that estimated. In this way, the code can be used as a tool for analyzing and interpreting radiation effects test data. After agreement has been obtained between the experimental and calculated results for a number of test conditions, the code can then be used to extend the test results to other test or operating conditions.

As an example of the results from this code, Fig. 3 shows predicted I-V curves for a particular solar cell for several fluences of 300-keV protons impinging on the illuminated surface. The parameters for the undamaged cell were adjusted to give agreement with the performance curve supplied by the manufacturer. The proton damage was simulated by a distribution of recombination centers, concentrated mainly in the region of the maximum range of the protons. If adequate test data for the proton fluences were available, the validity of the model for the proton damage could be tested by comparing experiment to prediction.

REFERENCES

1. Naber, J. A., Horiye, H., and van Lint, V. A. J., "Radiation Effects on Silicon," Final Report GA-8668, Gulf General Atomic, Inc., Aug. 20, 1968.

2. Naber, J. A., Horiye, H., and Berger, R. A., "Production and Annealing of Defects in Lithium-Diffused Silicon After 30-MeV Electron Irradiation at 300°K," Proceedings of the Conference of Effects of Lithium Doping on Silicon Solar Cells, held at the Jet Propulsion Laboratory, May 9, 1969, Technical Memorandum 33-435. Jet Propulsion Laboratory, Pasadena, Calif., Aug. 15, 1969.

3. Naber, J. A., Passenheim, B. C., and Berger, R. A., "Study of Radiation Effects in Silicon Solar Cells," Report No. GA-9909, Annual Report for Contract No. NAS 7-100, Gulf General Atomic, Inc., Jan. 23, 1970.

4. Naber, J. A., Passenheim, B. C., and Horiye, H., "Introduction and Annealing of Damage in Lithium-Diffused Silicon," Proceedings of the Third Annual Conference on Effects of Lithium Doping on Silicon Solar Cells, held at the Jet Propulsion Laboratory April 27 and 28, 1970, Technical Memorandum 33-467. Jet Propulsion Laboratory, Pasadena, Calif., April 1, 1971.

5. Passenheim, B. C., and Naber, J. A., Radiation Effects, Vol. 2, p. 229, 1970.

6. Passenheim, B. C., Naber, J. A., and Berger, R. A., "Production and Annealing of Defects in Lithium-Diffused Silicon After Irradiation With 30-MeV Electrons and Fission Neutrons at 300°K," Conference Record of the 8th IEEE Photovoltaic Specialists Conference, Seattle, Wash., Aug. 4-6, 1970, IEEE Catalog No. 70C-32 ED, pp. 260-266.

7. Naber, J. A., Horiye, H., and Passenheim, B. C., "Lithium-an Impurity of Interest in Radiation Effects in Silicon," to be published in Radiation Effects (1971).

8. Passenheim, B. C., et al., "Study of Radiation Effects in Silicon Solar Cells," Report No. Gulf-RT-10482, Annual Report for Contract No. NAS 7-100, Gulf Radiation Technology, Jan. 20, 1971.

9. Young, R. C., et al., J. Appl. Phys., Vol. 40, p. 271, 1968.

10. Shockley, W., and Read, W. T., Jr., Phys. Rev., Vol. 87, p. 835, 1952.

11. Lax, M., Phys. Rev., Vol. 119, p. 1502, 1960.

12. Leadon, R., and Naber, J. A., J. Appl. Phys., Vol. 40, p. 2633, 1969.

13. Damask, A. C., and Dienes, G. J., Point Defects in Metals, Gordon and Breach, Science Publishers, New York, 1963.

14. Pell, E. M., J. Appl. Phys., Vol. 31, p. 291, 1960.

15. Fuller, C. S., and Severiens, J. C., Phys. Rev., Vol. 96, p. 21, 1960.

16. Maita, J. P., J. Phys. Chem. Solids, Vol. 4, p. 68, 1958.

17. Leadon, R., and Vaughn, M., "Short-Pulsed Radiation Effects on Dynamic Electronic Components," Final Report on Contract DASA01-68-C-0123, DASA Report No. 2358 Defense Atomic Support Agency; also Gulf General Atomic Report GA-9397, June 5, 1969.

18. Leadon, R. E., et al., "Radiation Effects on Dynamic Electronic Components," Final Report on Contract DAOSA01-69-C-0113, DASA Report No. 2546 Defense Atomic Support Agency; also Gulf Radiation Technology Report GA-9775, July 1970.

Table 1. Summary of the results of isochronal and isothermal annealing experiments on electron- and neutron-irradiated lithium-diffused float-zone and quartz-crucible silicon

Sample type	Float zone			Quartz crucible		
Lithium donor density, Li/m^{-3}	2.5×10^{22}	4.5×10^{20}	2×10^{21}	2.5×10^{21}	4.5×10^{20}	2.5×10^{21}
Fluence (particles/m^2)	$\sim 10^{17}$	10^{16} to 10^{17}	5×10^{14}	1.5×10^{16} to 8×10^{16}	10^{16}	4×10^{14}
Radiation	30-MeV electrons	30-MeV electrons	Fission neutrons	30-MeV electrons	30-MeV electrons	Fission neutrons
Activation energy, eV	0.85 ±0.10	0.60 ±0.10	0.67 ±0.05	1.0 ±0.2	0.75 ±0.10	1.2 ±0.6
Frequency factor, sec^{-1}	$\sim 10^{10}$	Unknown	$\sim 10^{7}$	10^{8} to 10^{10}	10^{7} to 10^{8}	Unknown

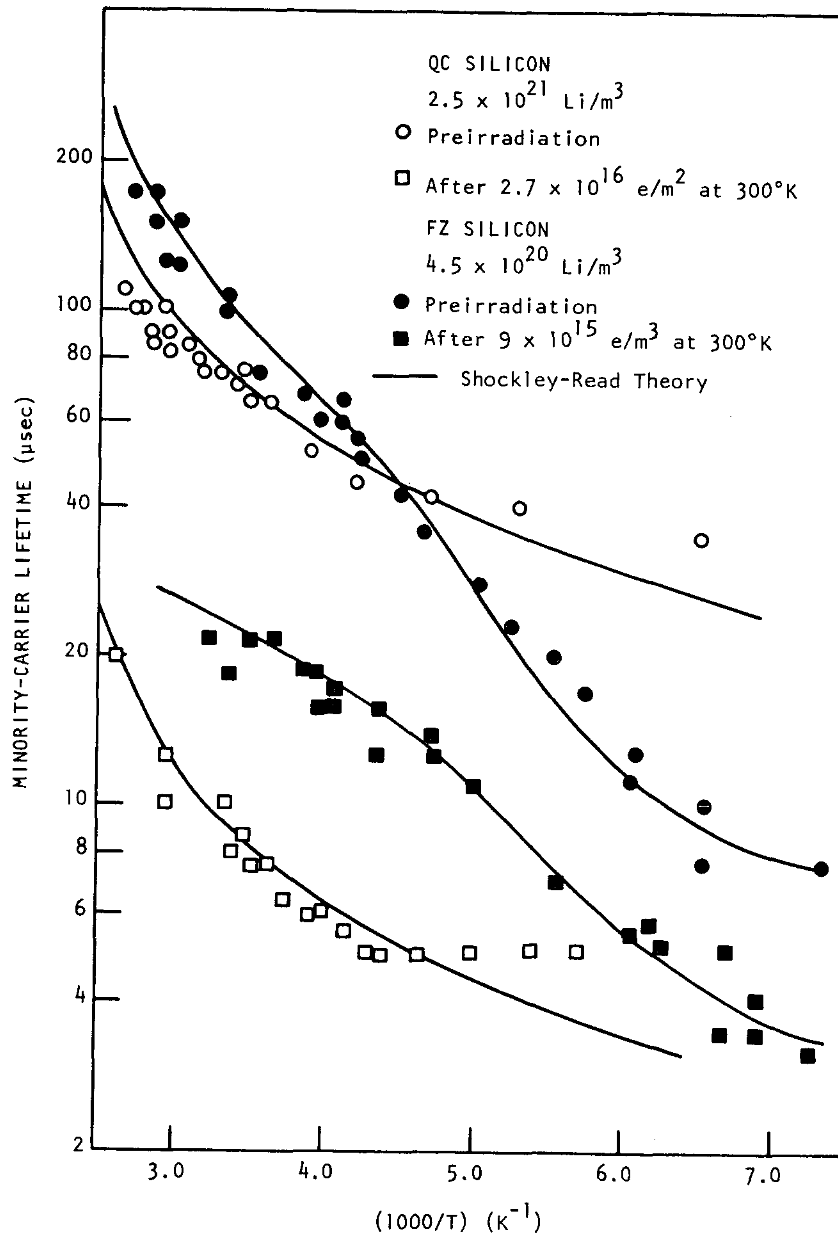

Fig. 1. Inverse temperature dependence of minority-carrier lifetime of lithium-diffused float-zone and quartz-crucible silicon before and after irradiation with 30-MeV electrons at room temperature

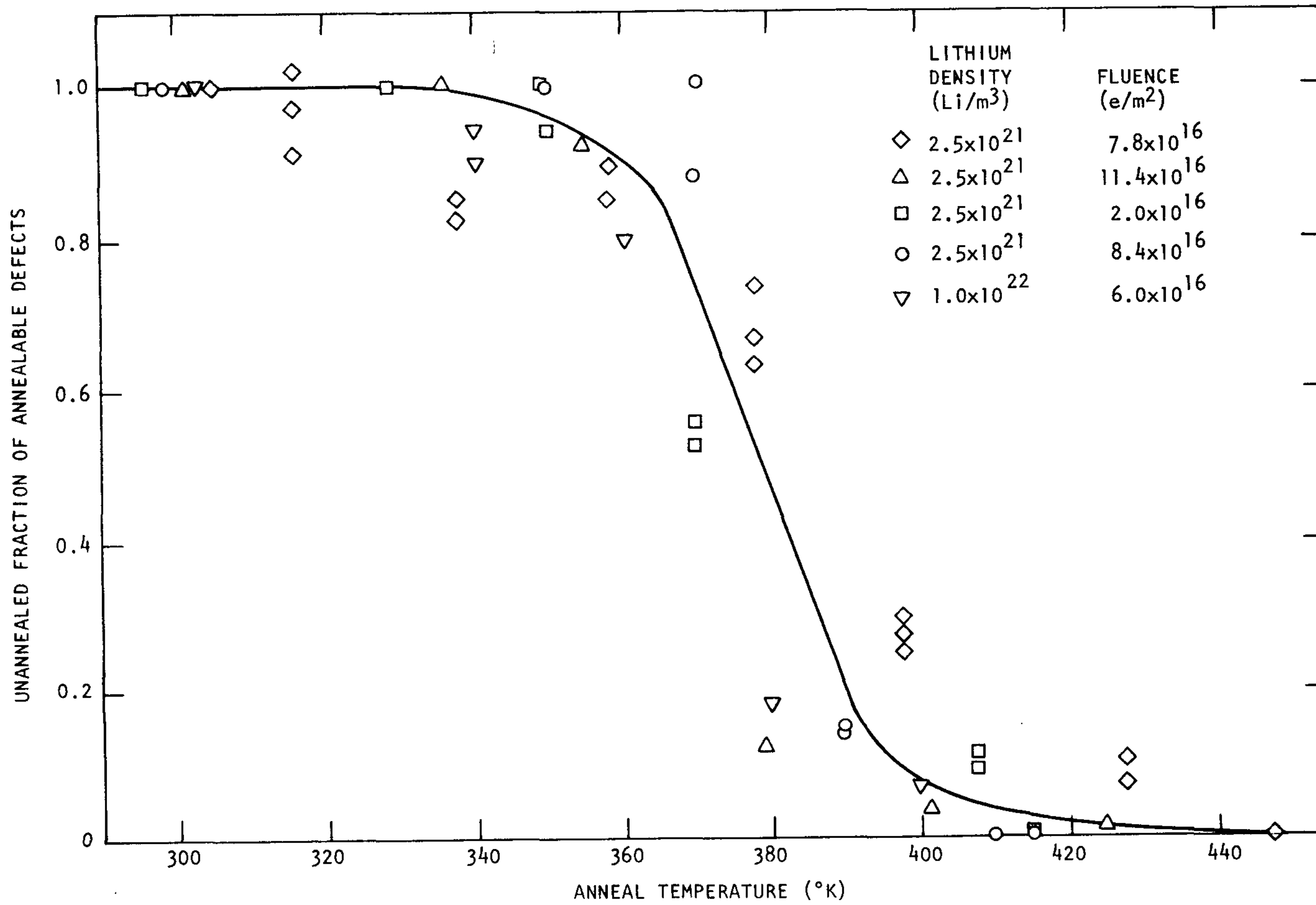

Fig. 2. Unannealed fraction of annealable defects after 5-min isochronal anneals at indicated temperatures after 30-MeV irradiation of lithium-diffused N-type QC silicon irradiated at 300 K

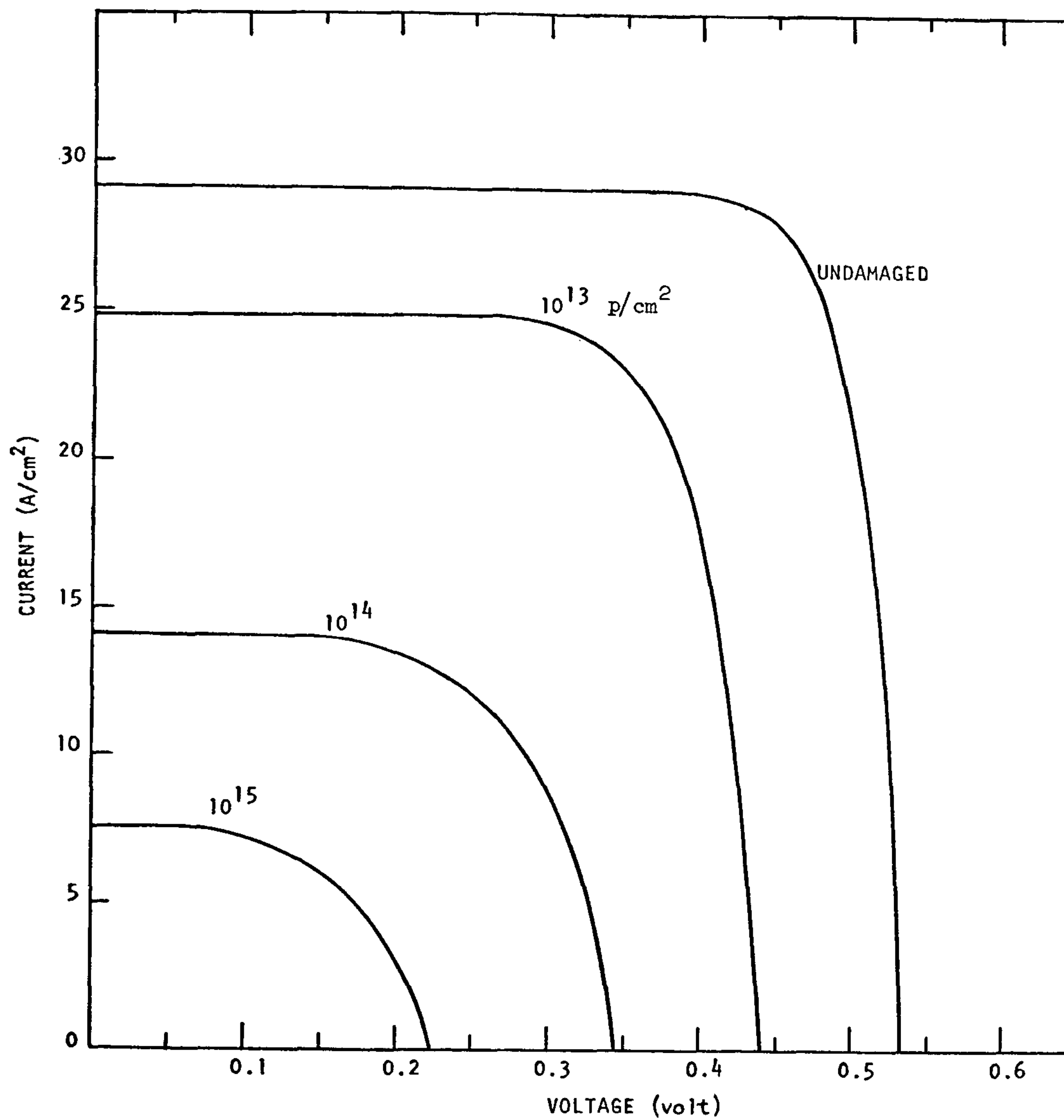

Fig. 3. Current-voltage curves of a graded-junction cell degraded by 300-keV protons to various fluences